AGU ADVANCING EARTH AND SPACE SCIENCES

Geophysical Research Letters

RESEARCH LETTER
10.1029/2025GL115260

On the Kinetic Energy Input of Magnetosheath Jets Into the Magnetosheath

Eva Krämer[1], Shahab Fatemi[1], Maria Hamrin[1], Herbert Gunell[1], and Gabriella Nordin[1]

[1]Department of Physics, Umeå University, Umeå, Sweden

Abstract Magnetosheath jets, plasma structures with enhanced dynamic pressure, are frequently observed in the terrestrial magnetosheath. However, their mass, momentum, and energy content are still unknown. We utilize Amitis, a 3D hybrid-kinetic plasma simulation, to study the mass, momentum, and energy content of jets in the subsolar magnetosheath. We also analyze the kinetic, thermal, and electromagnetic energy flux associated with jets. Jets comprise up to 21% of the quasi-parallel magnetosheath and can carry up to half of the kinetic energy. Furthermore, jets convert kinetic energy to thermal energy. Our hybrid simulations also suggest that while jets can form downstream of the quasi-perpendicular shock, their volume and energy content are much small compared to jets downstream of the quasi-parallel bow shock. We conclude that magnetosheath jets play a vital role in heating up the magnetosheath and significantly influence the dynamics of the quasi-parallel magnetosheath.

Plain Language Summary The solar wind is a supersonic plasma flow, continuously ejected from the Sun. It interacts with the Earth's magnetic field, leading to the formation of a collisionless shock front called the bow shock, where the solar wind is heated and compressed. The region downstream of the bow shock, the magnetosheath, contains decelerated, heated, and compressed solar wind plasma. Within the magnetosheath, plasma structures with significantly higher kinetic energy density occasionally form, known as magnetosheath jets. Using a three-dimensional hybrid plasma model (kinetic ions, fluid electrons), we quantify the mass, momentum, and energy carried by the jets in the subsolar magnetosheath. Our analysis focuses on the flux of kinetic energy associated with theses structures as they move into and out of the magnetosheath. The results show that, under conditions where the interplanetary magnetic field is closely aligned with the solar wind flow, jets play a dominant role in transporting plasma and driving dynamic processes in the quasi-parallel magnetosheath.

Key Points:

- Magnetosheath jets carry up to half of the kinetic energy in the quasi-parallel magnetosheath
- Jets transfer energy to the rest of the magnetosheath
- Jets downstream of quasi-perpendicular shocks are smaller and carry less energy than jets downstream of quasi-parallel shocks

Supporting Information:

Supporting Information may be found in the online version of this article.

Correspondence to:

E. Krämer,
eva.kramer@umu.se

Citation:

Krämer, E., Fatemi, S., Hamrin, M., Gunell, H., & Nordin, G. (2025). On the kinetic energy input of magnetosheath jets into the magnetosheath. *Geophysical Research Letters*, *52*, e2025GL115260. https://doi.org/10.1029/2025GL115260

Received 7 FEB 2025
Accepted 23 JUL 2025

Author Contributions:

Conceptualization: Eva Krämer, Shahab Fatemi, Maria Hamrin, Herbert Gunell
Formal analysis: Eva Krämer
Funding acquisition: Shahab Fatemi, Maria Hamrin
Investigation: Eva Krämer
Methodology: Eva Krämer, Shahab Fatemi, Maria Hamrin
Project administration: Maria Hamrin
Resources: Shahab Fatemi
Software: Shahab Fatemi
Supervision: Shahab Fatemi, Maria Hamrin, Herbert Gunell
Visualization: Eva Krämer
Writing – original draft: Eva Krämer
Writing – review & editing: Eva Krämer, Shahab Fatemi, Maria Hamrin, Herbert Gunell, Gabriella Nordin

1. Introduction

Bow shocks around planetary bodies heat, compress, and slow down the incoming solar wind plasma. At the Earth's bow shock, close to the subsolar point, the kinetic energy density is on average reduced by a factor of four according to the Rankine–Hugoniot jump conditions (e.g., Hietala et al., 2024). However, sometimes the kinetic energy density is less reduced, resulting in plasma structures with enhanced dynamic pressure (or equivalently, an enhancement in the dynamic pressure), known as magnetosheath jets (Plaschke et al., 2018; Krämer et al., 2024, and references therein). While jets are frequently observed in the terrestrial magnetosheath (e.g.., Archer & Horbury, 2013; Plaschke et al., 2013; Raptis et al., 2020), how much mass, momentum, and energy jets carry is still unknown. Using a 3D, hybrid-kinetic simulation of the solar wind interaction with Earth's magnetosphere at realistic scales (Fatemi et al., 2024) we aim to quantify this contribution.

The majority of magnetosheath jets are thought to form close to the bow shock (Plaschke et al., 2013) and propagate through the magnetosheath (Krämer et al., 2024; Plaschke et al., 2018, and references therein), with some fraction reaching the magnetopause (Plaschke et al., 2016). Jets are mostly observed downstream of the quasi-parallel shock (Archer & Horbury, 2013; Plaschke et al., 2013; Raptis et al., 2020; Vuorinen et al., 2019), the region of the shock where the angle between the bow shock normal and interplanetary magnetic field (IMF) is $<45°$ (e.g., Balogh et al., 2005, and references therein). In contrast, the quasi-perpendicular bow shock occurs where this angle exceeds $45°$ (Balogh et al., 2005). Correspondingly, the quasi-parallel (quasi-perpendicular) magnetosheath is the region magnetically connected to the quasi-parallel (quasi-perpendicular) bow shock (e.g., Karlsson et al., 2021).

Jet formation at the bow shock is an active field of research. For example, jet ripples (Hietala & Plaschke, 2013), foreshock compressive structures (Suni et al., 2021), and bow shock reformation (Raptis et al., 2022) are suggested to contribute to jet formation. Nevertheless, jets have also been observed downstream of the quasi-perpendicular shock (Goncharov et al., 2020) where they are suggested to be magnetic flux tubes connecting to the quasi-parallel bow shock, nonreconnecting current sheets, reconnection outflows, and/or mirror mode waves (Kajdič et al., 2021). Gyrating ion populations close to the bow shock might also lead to jet-like structures (Vuorinen et al., 2023).

Jets propagate through the magnetosheath, interacting with the surrounding plasma in various ways and transferring energy. One of those interaction mechanism is wave-particle interactions, which is known to transfer energy (Gunell et al., 2014; Karlsson et al., 2018; Krämer et al., 2023). Jets can also form bow waves ahead of them (Karimabadi et al., 2014) which accelerate electrons (Liu et al., 2019). Jets have been found to occur more often close to the bow shock (Plaschke et al., 2013) and have been suggested to dissipate energy as they move through the magnetosheath (Savin et al., 2008) and thermalize the plasma associated with jets (Karlsson et al., 2018). However, some jets can reach the magnetopause, and if they have large scale sizes, they can be geoeffective by, e.g., exciting ultra low frequency waves observable on the ground or causing auroral brightening (e.g., Norenius et al., 2021; Wang et al., 2018; Wang et al., 2022).

While these different interaction mechanisms of jets with the surrounding plasma are known, the amount of energy jets transfer through the magnetosheath remains uncertain. Instead of investigating single interaction mechanisms, such as wave-particle interaction, we take a different approach, and we explore a spatially confined region of the magnetosheath using the Amitis simulation (Fatemi et al., 2017). First, we explain our model and methods in Section 2. After that, in Section 3.1 we quantify the amount of the kinetic mass, momentum, and energy is stored in jets. Then, in Section 3.2, we calculate the energy flux through the boundaries of a confined magnetosheath region to determine the amount of energy converted into other forms. Finally, in Section 4 we summarize our results and discussion.

2. Methods

2.1. Simulation

To model the near-Earth plasma environment, we use Amitis, a time-dependent, 3D in velocity and configuration space, and grid-based plasma model that treats ions as super-particles and electrons as a massless, charged-neutralizing fluid. It has been recently upgraded to run on multi-GPU platforms (Fatemi et al., 2022) and has been successfully applied to study plasma interaction with Earth at realistic scales (Fatemi et al., 2024). We refer the reader to Fatemi et al. (2017) for a detailed description of the model principles and the involved equations.

The presented simulation results in this study use the following coordinate system: x is directed toward the sun, z is aligned with the magnetic pole pointing to the geographic north, and y completes the right-handed coordinate system. The solar wind flow is purely along the $-x$ axis. The simulation cells are a Cartesian cube of length 500 km. The inner magnetospheric boundary is a conductive sphere with a radius of 30000 km $\approx 4.7\mathrm{R_E}$ where $\mathrm{R_E} = 6371$ km is the Earth radius. The Earth magnetic dipole moment is 31.78 $\mu\mathrm{T}\cdot\mathrm{R_E}^3$, pointing along the $-z$ axis.

In this study, we use two simulation runs. One with an almost radial IMF ($B_{\mathrm{IMF}} = [+4.83, -1.30, 0.0]$ nT), denoted as RX (see S1 for an overview). RX corresponds to simulation R1Y described by Fatemi et al. (2024). The other run has a purely northward IMF ($B_{\mathrm{IMF}} = [0.0, 0.0, +5.0]$ nT), denoted as RZ (see S2), which has a similar setup to the simulations described by Fatemi et al. (2024). For both simulations, we only include solar wind protons with velocity $[-400, 0, 0]$ km/s, density 7 cm^{-3}, and temperature 10 eV. The solar wind dynamic pressure is 1.86 nPa. The solar wind protons are modeled as 15 macro-particles per cell. The Movie S1 and Movie S2 show the time development of the magnetic field, plasma density, electromagnetic energy density, and kinetic energy density for the RX and RZ run respectively. For the RX simulation, after the 8-min period we use in our analysis, the IMF orientation changes to a southward IMF through the passage of a current sheet (simulation R1S in Fatemi et al. (2024)). The transient period is not included in this study, and we only investigate the magnetosheath before the current sheet arrival at the bow shock, however, the current sheet does change the foreshock environment before interacting with the bow shock.

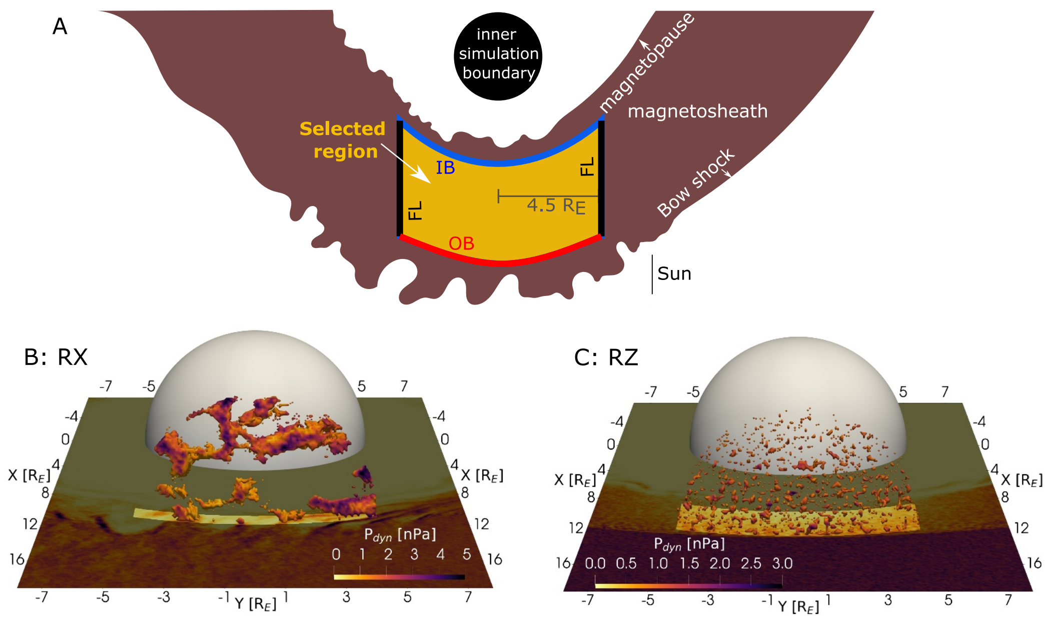

Figure 1. (a) Sketch of the selected magnetosheath region (yellow) in the *xy*-plane with the outer boundary (OB, red) and inner boundary (IB, blue) as partial spheres and the flanks (FL, black) restricted by $\sqrt{y^2 + z^2} < 4.5$ R$_\mathrm{E}$. (b) Dynamic pressure at the $z = 0$ plane at physical time 10:40 min for the RX simulation. We show the 3D structure of the magnetosheath jets. The white sphere represents the conducting boundary of the simulation at 4.7 R$_\mathrm{E}$. The view is from the Sun toward Earth. (c) Same as B at physical time 40:00 min for the RZ simulation with a different scale of the colorbar for better visibility.

2.2. Identification of Jets

First, we identify magnetosheath jets using a criterion similar to the one established by Plaschke et al. (2013), that is, $P_{\mathrm{dyn,x}} > 0.5 P_{\mathrm{dyn,sw}}$ with $P_{\mathrm{dyn,x}}$ the dynamic pressure in the magnetosheath using only v_x and $P_{\mathrm{dyn,sw}}$ the upstream solar wind dynamic pressure. This criterion, hereafter referred to as C1, should only be applied in the subsolar magnetosheath with solar zenith angles angles <30° (Plaschke et al., 2013).

However, the C1 criterion cannot reveal whether the excess kinetic energy is converted to other forms of energy or if jets are deflected in the magnetosheath. For example, consider a dynamic pressure enhancement with $v_x = C$, where $C \neq 0$, and $v_{y,z} = 0$. Let us assume that dynamic pressure enhancement is classified as a jet according to the C1 criterion. Now, if the velocity changes by deflection to $v_x = 0, v_{y,z} = C$ without any change in speed nor the dynamic pressure, the enhancement will not be classified as a jet under the C1 criterion anymore. However, since the dynamic pressure of the plasma entity did not change, no energy conversion has occurred, and the change is only due to the plasma flow deflection. While such drastic changes in the velocity are unrealistic, gradual changes in the velocity from parallel to perpendicular to the Sun–Earth line are expected due to the deflection of magnetosheath plasma around Earth.

To assess the amount of energy jets convert, we investigate dynamic pressure enhancements that fulfill $P_{\mathrm{dyn}} > 0.5\ P_{\mathrm{dyn,sw}}$. Here P_{dyn} is calculated using the magnitude of the plasma flow velocity, $|v|$, instead of its component along the *x*-axis, v_x. We refer to the criterion as the C2 criterion.

We restrict our analysis to a confined region in the subsolar magnetosheath. This confined region is illustrated in yellow in Figure 1a. The boundaries of this region are the outer boundary (OB, red), inner boundary (IB, blue), and the flanks (FL, black) (Figure 1a). The IB and OB are approximated as partial spheres in the subsolar magnetosphere and the FL are chosen such that the solar zenith angle <30° to fulfill the C1 criterion. The criteria for each boundary are given in Appendix A.

Figures 1b and 1c show the confined magnetosheath region and the contours for jets, obtained from the C1 criterion for both simulation runs. Figure 1b shows jets in the subsolar magnetosheath of the RX simulation downstream of a quasi-parallel shock. These jets are interconnected structures as described by Fatemi et al. (2024)

10.1029/2025GL115260

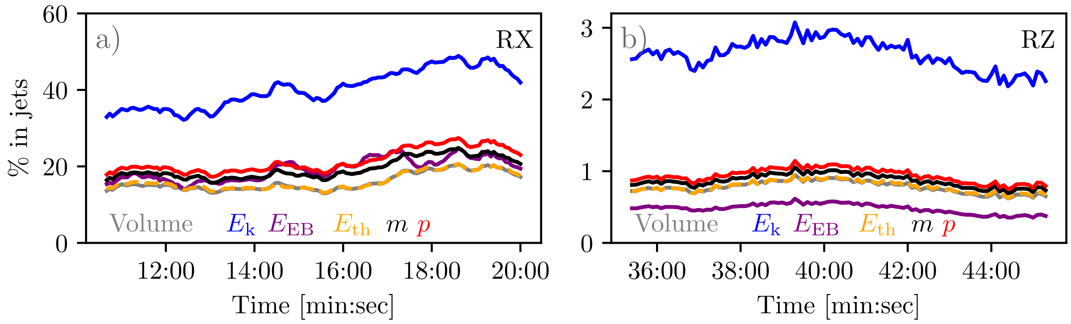

Figure 2. The relative kinetic energy E_k (blue), electromagnetic energy E_{EB} (purple), thermal energy E_{th} (orange), mass m (black), and momentum p (red) content in magnetosheath jets (C1 criterion). The percentage of the magnetosheath volume classified as jet is shown in gray. (a) RX simulation, (b) RZ simulation. Note the different scales for the vertical axis.

and Ren et al. (2024). Figure 1c shows jets in the RZ simulation downstream of a quasi-perpendicular shock. These jets are much smaller and unlike those downstream of the quasi-parallel shock, they are not interconnected structures. Their sizes, however, are comparable to the simulation cell sizes, and therefore, their actual size might be smaller than those shown in Figure 1b. Jets downstream of the quasi-perpendicular shock in our RZ simulation only exist close to the bow shock which suggests that they could be attributed to the gyrating ion motion described by Vuorinen et al. (2019). These jets are not associated to flux tubes connected to the quasi-parallel shock, nonreconnecting current sheets, or reconnection outflows as suggested by Kajdič et al. (2021). However, investigating the origin of quasi-perpendicular jets will be conducted in a separate study.

3. Results

We first quantify the mass, momentum, and energy carried by jets in the magnetosheath. We then investigate the amount of the flux moving through the boundaries of the magnetosheath region that is associated with jets.

3.1. Mass, Momentum, and Energy Content in Jets

The proportion of the magnetosheath volume that is classified as jets (gray) is shown in Figure 2 as well as the proportions of mass (black), momentum (red), kinetic energy (blue), electromagnetic energy (purple), and thermal energy (orange) carried by these jets in the RX (Figure 2a) and RZ simulations (Figure 2b). In the RX simulation, jets occupy approximately 16% (and up to 21%) of the magnetosheath volume, while in the RZ run, this fraction is significantly lower at <1%.

For the RX (RZ) simulation, jets carry up to 49% (3.1%) of the kinetic bulk energy, 25% (0.6%) of the electromagnetic energy, 21% (1.0%) of the thermal energy, 27% (1.1%) of the bulk momentum, and 25% (1.1%) of the mass of the magnetosheath. The kinetic energy proportion of jets is approximately double their volume proportion in the RX simulation and three times their volume proportion in the RZ simulation. This finding is consistent with the identification criterion that requires an increased kinetic energy density compared to the average dynamic pressure in the magnetosheath. Note that the vertical axes in Figure 2 have different scales.

For the RX simulation, all the investigated properties increase over time, likely due to stable upstream conditions, leading to a more stable foreshock. Earlier observations and simulations suggest that a stable foreshock results in the formation of more jets (Archer & Horbury, 2013). Around 19:00, the volume of jets starts to decrease again, likely due to the approaching current sheet disturbing the foreshock. In contrast, for RZ, the jet volume and energy remain roughly constant over time.

We conclude that jets carry a significant proportion of the energy in the magnetosheath downstream of the quasi-parallel bow shock but not downstream of the quasi-perpendicular bow shock, as more jets are identified in the quasi-parallel magnetosheath. This result agrees with previous studies that found that magnetosheath jets are more often observed downstream of the quasi-parallel bow shock compared to the quasi-perpendicular bow shock (e.g., Archer & Horbury, 2013; Plaschke et al., 2013).

10.1029/2025GL115260

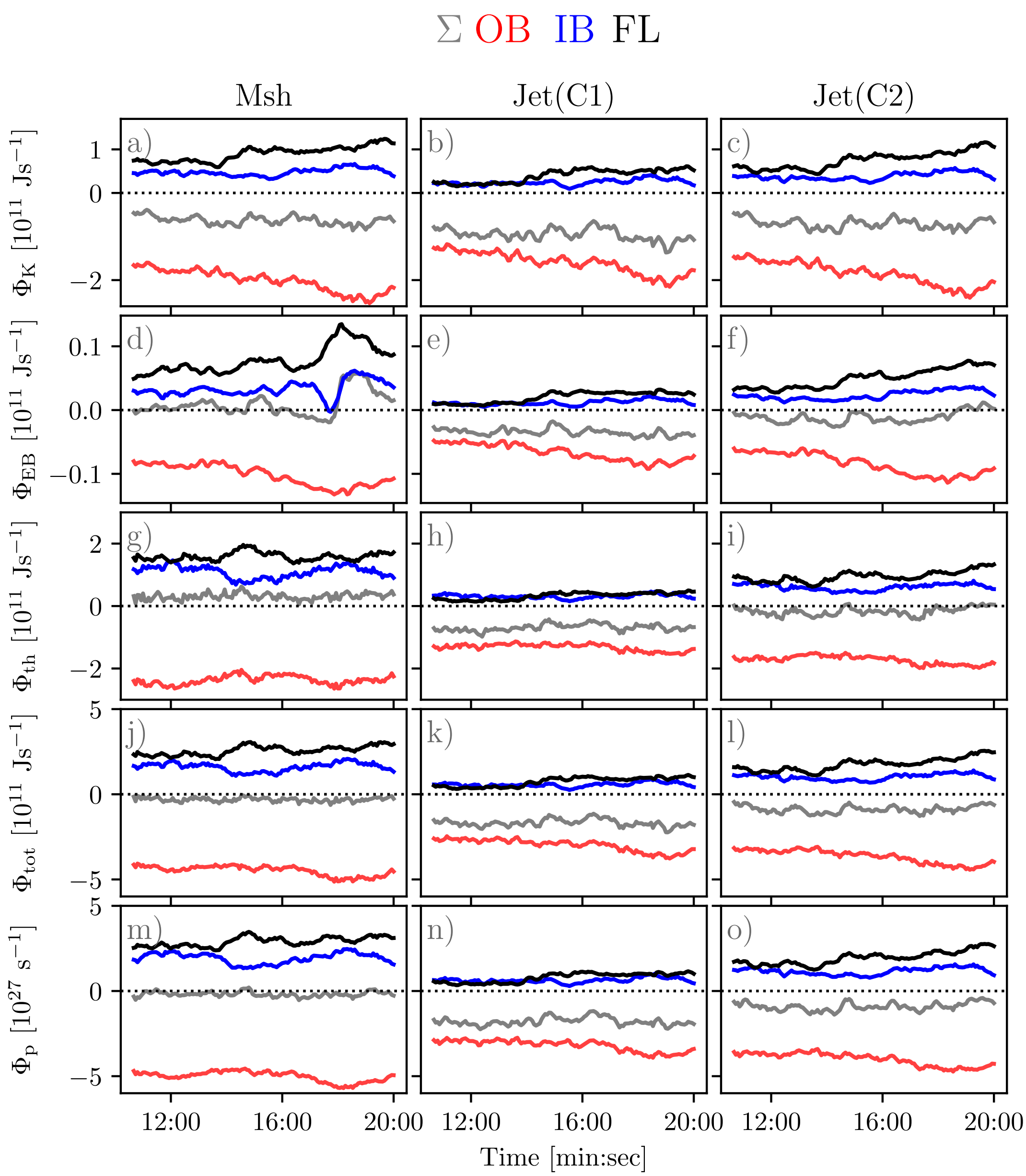

Figure 3. Kinetic energy flux Φ_K, electromagnetic energy flux Φ_{EB}, thermal energy flux Φ_{th}, total energy flux Φ_{tot}, and particle flux Φ_p into and out of the selected magnetosheath region through the outer boundary (OB, red), inner boundary (IB, blue), the flanks (FL, black), and the sum off all boundaries (Σ, gray) for RX. (a) Φ_K for flux crossing the boundaries, (b) Φ_K using the C1 criterion, (c) Φ_K using the C2 criterion, d–f: same as a–c for Φ_{EB}, g–i: same as a–c for Φ_{th}, j–l: same as a–c for Φ_{tot}, m–o: same as a–c for Φ_p. Negative flux is defined as incoming while positive flux is defined as outgoing from the boundary. Note the different scales for the vertical axes.

3.2. Energy Flux

We investigate jets' contribution to the kinetic, electromagnetic, and thermal energy flux across the boundaries (OB, IB, FL) of the selected region. Our results are presented in Figure 3 which shows the integrated kinetic energy flux Φ_K (Figures 3a–3c), integrated electromagnetic energy flux Φ_{EB} (Figures 3d–3f), integrated thermal energy flux Φ_{th} (Figures 3g–3i), and total integrated energy flux $\Phi_{tot,A} = \Phi_{kin,A} + \Phi_{EB,A} + \Phi_{th,A}$ with $A \in \{OB, IB, FL, \Sigma\}$ (Figures 3j–3l) across the magnetosheath boundaries for RX. With Σ we refer to the sum of the different integrated energy fluxes over all boundaries, $\Phi_{X,\Sigma} = \Phi_{X,OB} + \Phi_{X,IB} + \Phi_{X,FL}$ with $X \in \{K, EB, th, tot\}$. The first column shows the integrated energy flux of all magnetosheath plasma crossing the boundaries (Msh), the second column only flux of C1 jets, and the third column only flux of C2 jets. With integrated flux, we refer to integration over the respective boundary surface of the selected magnetosheath region. We show the different integrated flux for the OB (red), the IB (blue), and the FL (black) as well as Σ (gray). Negative flux is defined as incoming while positive flux is outgoing from the selected magnetosheath region. The integrated kinetic energy flux at the OB is incoming ($\Phi_K < 0$), while the flux at the IB and at the flanks are outgoing ($\Phi_K > 0$). Additionally, Figures 3m–3o shows the integrated particle flux Φ_p following the same nomenclature as for the energy fluxes.

The energy flux across the selected region is approximately conserved, $\Phi_{\Sigma,\mathrm{tot}} \approx 0$ (gray line in Figure 3j). $\Phi_{\Sigma,\mathrm{tot}}$ is, on average, slightly smaller than 0 which is an effect of the region being not strictly stationary over different simulation time steps and the shape of the selected region. $\Phi_{EB,\Sigma}$ (gray line in Figure 3d) fluctuates around 0 over time and overall the electromagnetic energy flux is small compared to the thermal and kinetic energy flux ($\Phi_{EB,OB} \ll \Phi_{K/th,OB}$). Overall, the kinetic energy is a source of energy ($\Phi_{K,\Sigma} < 0$, gray line in Figure 3a) while the thermal energy is a sink ($\Phi_{th,\Sigma} > 0$, gray line in Figure 3g). We can therefore conclude that the kinetic energy is primarily converted to thermal energy in the magnetosheath.

To assess the role of jets in modulating the energy flux across the magnetosheath, we analyze the contributions from C1 and C2 jets, which reveal a net inflow of energy into the region (gray lines in Figures 3k and 3l). On average, C1 jets input 37% of the total incoming energy flux through the OB ($\Phi_{\mathrm{tot},\Sigma,C1}/\Phi_{\mathrm{tot,OB,msh}}$), while C2 input 20%. This inflow encompasses kinetic, thermal, and electromagnetic energy (gray lines in Figures 3b, 3c, 3e, 3f, 3h, and 3i), with kinetic energy being the dominant component ($\Phi_{\mathrm{kin},\Sigma,C1}/\Phi_{\mathrm{tot},\Sigma,C1} = 57\%$, $\Phi_{\mathrm{kin},\Sigma,C2}/\Phi_{\mathrm{tot},\Sigma,C2} = 82\%$). This finding aligns with the definition of magnetosheath jets as localized enhancements in kinetic energy density. As jets propagate through the magnetosheath, they may degrade due to the loss of excess kinetic energy, which is then transferred to the ambient plasma, contributing to the overall energy budget.

Overall, C1 jets carry more energy into the magnetosheath compared to C2 jets, which reflects the previously discussed peculiarity of the C1 criterion (see discussion in Section 2.2). Consequently, the use of the C1 criterion results in overestimating the converted energy and should not be employed for investigating energy transfer by jets. The C2 criterion, however, gives a more realistic estimate for the proportion of the net energy flux, assuming that the conversion rate is the same for all dynamic pressure thresholds. Not all jets lose their identity in the selected volume, since there is an outflow of kinetic energy in jets through the FL and IB (Figure 3c). Jets that move through the flanks will likely continue to move along with the magnetosheath flow around Earth. Jets that move through the IB can impact the magnetopause and potentially be geoeffective, for example, triggering ULF waves (Norenius et al., 2021; Wang et al., 2022). This shows that a significant amount of jets traverse the magnetosheath and impact the magnetopause on a regular basis. This finding agrees with Plaschke et al. (2020).

An outstanding question concerns the fate of the excess kinetic, thermal, and electromagnetic energy carried by jets. Jets lose, on average, 38% of their kinetic energy ($\Phi_{\mathrm{kin},\Sigma,C2}/\Phi_{\mathrm{kin,OB,C2}}$), 14% of their electromagnetic energy ($\Phi_{EB,\Sigma,C2}/\Phi_{EB,OB,C2}$), and 10% of their thermal energy ($\Phi_{th,\Sigma,C2}/\Phi_{th,OB,C2}$). In comparison, net particle flux in jets corresponds to 23% of the incoming particle flux in jets at the OB ($\Phi_{p,\Sigma,C2}/\Phi_{p,OB,C2}$). The net inflow of particles due to jets indicates that jets degrade as they traverse the magnetosheath. In addition to degradation, reductions in average density and velocity likely contribute to the observed decrease in particle flux. As jets degrade, energy initially associated with them at the OB may no longer be attributed to the jet population at the IB or FL, instead appearing as a source of energy. This apparent energy gain is a consequence of jet propagation and degradation, rather than a definitive indicator of internal energy conversion. However, the degree of energy loss differs across energy forms. The smaller reduction in thermal energy flux compared to particle flux implies that jet temperatures increase during propagation. The loss of electromagnetic energy is likely attributable to the reduced volume of jets closer to the IB. The loss in kinetic energy in jets exceeds the loss of particles and therefore also the loss of jet volume. This additional loss of energy can therefore not only be attributes to the loss of jet volume but additional energy exchange mechanisms act on the jet plasma. Parts of the excess kinetic energy need to be converted to thermal energy, contributing to the overall thermal energy gain in the magnetosheath. Moreover, energy exchange with the surrounding plasma may occur through bow waves ahead of the jets (Liu et al., 2019, 2020), wave–particle interactions (Gunell et al., 2014; Karlsson et al., 2018; Krämer et al., 2023) and superdiffusion (Savin et al., 2008).

10.1029/2025GL115260

We repeated the analysis for RN, which yielded similar results (see S3). However, the overall contribution of jets is less pronounced due to their relatively small volume (Figure 2b). Since jets are confined to areas near the bow shock and lose their identity further downstream (see Figure 1c), they serve as localized sources of kinetic, electromagnetic, and thermal energy in the magnetosheath.

4. Summary

We used the 3D hybrid-kinetic simulation Amitis to investigate the mass, momentum, and energy content in magnetosheath jets. We also calculated the energy flux carried by jets crossing the boundaries of the subsolar magnetosheath. Our main findings and conclusions can be summarized as follows:

1. Up to approximately 20% of the magnetosheath downstream of the quasi-parallel bow shock can be classified as magnetosheath jets during stable IMF conditions.
2. Magnetosheath jets carry significant proportions of mass, momentum, and energy in the quasi-parallel magnetosheath.
3. Jets carry kinetic energy into the magnetosheath. Some of the excess kinetic energy is converted to thermal energy and therefore contributes to heating.
4. Jets downstream of the quasi-perpendicular bow shock are much smaller and exist only close to the bow shock compared to jets downstream of the quasi-parallel shock. They do not carry significant proportions of mass, momentum, and energy compared to the quasi-perpendicular magnetosheath.
5. Jet criteria that use only a velocity component, rather than speed, overestimate the energy (kinetic and electromagnetic) transferred to the magnetosheath. This is because they do not consider the deflection of magnetosheath plasma around the planet.

Our findings show the relevance of jets in the quasi-parallel magnetosheath where they make up a large part of the plasma volume and carry a significant proportion of mass, momentum and energy. As those jets move across the magnetosheath they convert their kinetic excess energy to thermal energy. To understand the relevant mechanisms of jets in the magnetosheath, further studies are needed focusing on the micro-physics involved, such as wave-particle interaction and turbulence.

Appendix A: Identification of the Confined Magnetosheath Region

This section details the selection of the confined region in the subsolar magnetosheath and its boundaries. The quasi-parallel bow shock is not well defined due various foreshock structures (Eastwood et al., 2005). Fatemi et al. (2024) showed that the magnetopause and bow shock models by Chao et al. (2002) do not represent the respective boundaries well for the RX simulations. To calculate the flux across a boundary, we also need to determine the normal of the boundary. The bow shock and magnetopause detection method used by Fatemi et al. (2024) does not identify magnetosheath boundaries with a well defined normal direction for RX. We therefore do not use the magnetopause and bow shock as the boundaries of the confined magnetosheath region. Instead, we employ the following strategy to define a IB, OB, and flank (FL) of a confined region in the subsolar magnetosheath:

1. We limit our analysis to the region where $r_{yz} = \sqrt{y^2 + z^2} < 4.5\mathrm{R_E}$ to ensure the applicability of the C1 criterion. This boundary, defining a cylinder, we refer to as the flank (FL).
2. We determine the bow shock and magnetopause location using the criteria described by Fatemi et al. (2024). Both boundaries need to satisfy: (a) the plasma density should be twice the upstream value, (b) the velocity should be 2/3 of the upstream value, and (c) the electric current should exceed 3 nA/m^2 for the bow shock and 9 nA/m^2 for the magnetopause.
3. For the subsolar magnetosheath, we approximate the bow shock and the magnetopause as partial spherical shells centered at (0,0,0). We calculate the median radius of the bow shock r_{bs} and magnetopause r_{mp} as well as their standard deviations, σ_{bs} and σ_{mp}.
4. We set the radius of the OB as $r_{OB} = r_{bs} - \sigma_{bs} - 3\mathrm{d}r$ with the grid cell size dr. The margin $\sigma_{bs} + 3\mathrm{d}r$ is used to make sure that unshocked solar wind plasma is not included, which would be misclassified as a jet.
5. We set the radius of the IB as $r_{IB} = r_{mb} + \sigma_{mp} + \mathrm{d}r$. The minimum distance of the IB is around 9 $\mathrm{R_E}$ which justifies the choice of $\sqrt{y^2 + z^2} < 4.5\ \mathrm{R_E}$. We also include a margin for the IB to exclude any magnetospheric plasma.

Due to the magnetospheric dynamics, the location of the magnetopause and bow shock boundaries vary over time. We therefore repeat the above steps for every time step of the simulation where simulation data is available.

We also calculate the flux across each boundary enclosing the investigated magnetosheath region. All boundaries are 500 km thick, corresponding to one grid cell. The boundaries satisfy $r_{\text{boundary}} < r < r_{\text{boundary}} + \mathrm{d}r$ with $r_{\text{boundary}} \in \{r_{OB}, r_{IB}, r_{yz}\}$.

Data Availability Statement

The simulation data for both simulation runs is available at https://doi.org/10.5281/zenodo.14724584 (Krämer et al., 2025).

Acknowledgments
E. Krämer, M. Hamrin, and G. Nordin were supported by Vetenskapsrådet (VR) 2018–03623 and by the Swedish National Space Agency (SNSA) Grant 2022-00138. S. Fatemi acknowledges financial support from SNSA, Grant 2022-00183. H. Gunell was supported by the SNSA Grant 2023-00208. The simulations were carried out using the EuroHPC JU Regular Access, grant EHPC-REG-2023R03-023. The data handling were enabled by resources provided by the National Academic Infrastructure for Supercomputing in Sweden (NAISS), through grants NAISS 2024/6-163 and 2024/4-5.

References

Archer, M., & Horbury, T. (2013). Magnetosheath dynamic pressure enhancements: Occurrence and typical properties. *Annales Geophysicae*, *31*(2), 319–331. https://doi.org/10.5194/angeo-31-319-2013

Balogh, A., Schwartz, S., Bale, S., Balikhin, M., Burgess, D., Horbury, T., et al. (2005). Cluster at the bow shock: Introduction. In *Outer magnetospheric boundaries: Cluster results* (pp. 155–160).

Chao, J., Wu, D., Lin, C.-H., Yang, Y.-H., Wang, X., Kessel, M., et al. (2002). Models for the size and shape of the Earth's magnetopause and bow shock. In *Cospar colloquia series* (Vol. 12, pp. 127–135). https://doi.org/10.1016/s0964-2749(02)80212-8

Eastwood, J., Lucek, E., Mazelle, C., Meziane, K., Narita, Y., Pickett, J., & Treumann, R. (2005). The foreshock. *Space Science Reviews*, *118*, 41–94.

Fatemi, S., Hamrin, M., Krämer, E., Gunell, H., Nordin, G., Karlsson, T., & Goncharov, O. (2024). Unveiling the 3d structure of magnetosheath jets. *Monthly Notices of the Royal Astronomical Society*, *531*(4), 4692–4713. https://doi.org/10.1093/mnras/stae1456

Fatemi, S., Poppe, A., Vorburger, A., Lindkvist, J., & Hamrin, M. (2022). Ion dynamics at the magnetopause of ganymede. *Journal of Geophysical Research: Space Physics*, *127*(1), e2021JA029863. https://doi.org/10.1029/2021ja029863

Fatemi, S., Poppe, A. R., Delory, G. T., & Farrell, W. M. (2017). Amitis: A 3d gpu-based hybrid-pic model for space and plasma physics. In *Journal of Physics: Conference Series* (Vol. 837). https://doi.org/10.1088/1742-6596/837/1/012017

Goncharov, O., Gunell, H., Hamrin, M., & Chong, S. (2020). Evolution of high-speed jets and plasmoids downstream of the quasi-perpendicular bow shock. *Journal of Geophysical Research: Space Physics*, *125*(6), e2019JA027667. https://doi.org/10.1029/2019ja027667

Gunell, H., Stenberg Wieser, G., Mella, M., Maggiolo, R., Nilsson, H., Darrouzet, F., et al. (2014). Waves in high-speed plasmoids in the magnetosheath and at the magnetopause. In *Annales Geophysicae* (Vol. 32(8), pp. 991–1009). https://doi.org/10.5194/angeo-32-991-2014

Hietala, H., & Plaschke, F. (2013). On the generation of magnetosheath high–speed jets by bow shock ripples. *Journal of Geophysical Research: Space Physics*, *118*(11), 7237–7245. https://doi.org/10.1002/2013ja019172

Hietala, H., Trotta, D., Fedeli, A., Wilson III, L., Vuorinen, L., & Coburn, J. (2024). Candidates for downstream jets at interplanetary shocks. *Monthly Notices of the Royal Astronomical Society*, *531*(2), 2415–2421. https://doi.org/10.1093/mnras/stae1294

Kajdič, P., Raptis, S., Blanco-Cano, X., & Karlsson, T. (2021). Causes of jets in the quasi-perpendicular magnetosheath. *Geophysical Research Letters*, *48*(13), e2021GL093173. https://doi.org/10.1029/2021gl093173

Karimabadi, H., Roytershteyn, V., Vu, H., Omelchenko, Y., Scudder, J., Daughton, W., et al. (2014). The link between shocks, turbulence, and magnetic reconnection in collisionless plasmas. *Physics of Plasmas*, *21*(6), 062308. https://doi.org/10.1063/1.4882875

Karlsson, T., Plaschke, F., Hietala, H., Archer, M., Blanco-Cano, X., Kajdič, P., et al. (2018). Investigating the anatomy of magnetosheath jets–mms observations. In *Annales Geophysicae* (Vol. 36(2), pp. 655–677). https://doi.org/10.5194/angeo-36-655-2018

Karlsson, T., Raptis, S., Trollvik, H., & Nilsson, H. (2021). Classifying the magnetosheath behind the quasi-parallel and quasi-perpendicular bow shock by local measurements. *Journal of Geophysical Research: Space Physics*, *126*(9), e2021JA029269. https://doi.org/10.1029/2021ja029269

Krämer, E., Fatemi, S., Hamrin, M., Gunell, H., & Nordin, G. (2025). Amitis simulation data [dataset]. *Zenodo*. https://doi.org/10.5281/zenodo.14724584

Krämer, E., Hamrin, M., Gunell, H., Karlsson, T., Steinvall, K., Goncharov, O., & André, M. (2023). Waves in magnetosheath jets—Classification and the search for generation mechanisms using mms burst mode data. *Journal of Geophysical Research: Space Physics*, *128*(7), e2023JA031621. https://doi.org/10.1029/2023ja031621

Krämer, E., Koller, F., Suni, J., LaMoury, A. T., Pöppelwerth, A., Glebe, G., et al. (2024). Jets downstream of collisionless shocks: Recent discoveries and challenges. *Space Science Reviews*, *221*(1), 1–59. https://doi.org/10.1007/s11214-024-01129-3

Liu, T. Z., Hietala, H., Angelopoulos, V., Omelchenko, Y., Roytershteyn, V., & Vainio, R. (2019). Themis observations of particle acceleration by a magnetosheath jet-driven bow wave. *Geophysical Research Letters*, *46*(14), 7929–7936. https://doi.org/10.1029/2019gl082614

Liu, T. Z., Hietala, H., Angelopoulos, V., Omelchenko, Y., Vainio, R., & Plaschke, F. (2020). Statistical study of magnetosheath jet-driven bow waves. *Journal of Geophysical Research: Space Physics*, *125*(7), e2019JA027710. https://doi.org/10.1029/2019ja027710

Norenius, L., Hamrin, M., Goncharov, O., Gunell, H., Opgenoorth, H., Pitkänen, T., et al. (2021). Ground-based magnetometer response to impacting magnetosheath jets. *Journal of Geophysical Research: Space Physics*, *126*(8), e2021JA029115. https://doi.org/10.1029/2021ja029115

Plaschke, F., Hietala, H., & Angelopoulos, V. (2013). Anti-sunward high-speed jets in the subsolar magnetosheath. In *Annales Geophysicae* (Vol. 31(10), pp. 1877–1889). https://doi.org/10.5194/angeo-31-1877-2013

Plaschke, F., Hietala, H., Angelopoulos, V., & Nakamura, R. (2016). Geoeffective jets impacting the magnetopause are very common. *Journal of Geophysical Research: Space Physics*, *121*(4), 3240–3253. https://doi.org/10.1002/2016ja022534

Plaschke, F., Hietala, H., Archer, M., Blanco-Cano, X., Kajdič, P., Karlsson, T., et al. (2018). Jets downstream of collisionless shocks. *Space Science Reviews*, *214*(5), 1–77. https://doi.org/10.1007/s11214-018-0516-3

Plaschke, F., Hietala, H., & Vörös, Z. (2020). Scale sizes of magnetosheath jets. *Journal of Geophysical Research: Space Physics*, *125*(9), e2020JA027962. https://doi.org/10.1029/2020ja027962

Raptis, S., Karlsson, T., Plaschke, F., Kullen, A., & Lindqvist, P.-A. (2020). Classifying magnetosheath jets using mms: Statistical properties. *Journal of Geophysical Research: Space Physics*, *125*(11), e2019JA027754. https://doi.org/10.1029/2019ja027754

Raptis, S., Karlsson, T., Vaivads, A., Pollock, C., Plaschke, F., Johlander, A., et al. (2022). Downstream high-speed plasma jet generation as a direct consequence of shock reformation. *Nature Communications*, *13*(1), 598. https://doi.org/10.1038/s41467-022-28110-4

Ren, J., Guo, J., Lu, Q., Lu, S., Gao, X., Ma, J., & Wang, R. (2024). Honeycomb-like magnetosheath structure formed by jets: Three-dimensional global hybrid simulations. *Geophysical Research Letters*, *51*(12), e2024GL109925. https://doi.org/10.1029/2024gl109925

Savin, S., Amata, E., Zelenyi, L., Budaev, V., Consolini, G., Treumann, R., et al. (2008). High energy jets in the Earth's magnetosheath: Implications for plasma dynamics and anomalous transport. *JETP letters*, *87*(11), 593–599. https://doi.org/10.1134/s0021364008110015

Suni, J., Palmroth, M., Turc, L., Battarbee, M., Johlander, A., Tarvus, V., et al. (2021). Connection between foreshock structures and the generation of magnetosheath jets: Vlasiator results. *Geophysical Research Letters*, *48*(20), e2021GL095655. https://doi.org/10.1029/2021gl095655

Vuorinen, L., Hietala, H., LaMoury, A. T., & Plaschke, F. (2023). Solar wind parameters influencing magnetosheath jet formation: Low and high imf cone angle regimes. *Journal of Geophysical Research: Space Physics*, *128*(10), e2023JA031494. https://doi.org/10.1029/2023ja031494

Vuorinen, L., Hietala, H., & Plaschke, F. (2019). Jets in the magnetosheath: Imf control of where they occur. In *Annales Geophysicae* (Vol. 37(4), pp. 689–697). https://doi.org/10.5194/angeo-37-689-2019

Wang, B., Nishimura, Y., Hietala, H., & Angelopoulos, V. (2022). Investigating the role of magnetosheath high-speed jets in triggering dayside ground magnetic ultra-low frequency waves. *Geophysical Research Letters*, *49*(22), e2022GL099768. https://doi.org/10.1029/2022gl099768

Wang, B., Nishimura, Y., Hietala, H., Lyons, L., Angelopoulos, V., Plaschke, F., et al. (2018). Impacts of magnetosheath high-speed jets on the magnetosphere and ionosphere measured by optical imaging and satellite observations. *Journal of Geophysical Research: Space Physics*, *123*(6), 4879–4894. https://doi.org/10.1029/2017JA024954